Modelling and fabrication of porous sandwich layer barium titanate with improved piezoelectric energy harvesting figures of merit

J. I. Roscow [a], R. W. C. Lewis [b], J. Taylor [c] and C. R. Bowen [a]

[a] Materials and Structures Centre, Department of Mechanical Engineering, University of Bath, Bath, BA2 7AY

[b] Renishaw Plc., Wotton Road, Charfield, Wotton-under-Edge, GL12 8SP

[c] Department of Electronic and Electrical Engineering, University of Bath, Bath, BA2 7AY

Keywords: Piezoelectric; Energy harvesting; Porosity; Microstructure; Finite element analysis.

Abstract

This paper demonstrates that porous 'sandwich' structures can provide an effective route for the design and optimisation of piezoelectric materials for energy harvesting applications, which is becoming an increasingly important technology for self-powered wireless networks and sensors. A numerical model is presented that accounts for the complex poling distribution throughout a layered ferroelectric and helps to develop a detailed understanding of the relationship between the geometry of the porous structure and the poling characteristics of porous ferroelectric materials, with good agreement with experimental data. Novel layered barium titanate ceramics were fabricated whereby dense outer layers surround a highly porous sandwich layer, and for specific layer geometries an unusual condition was achieved where the longitudinal piezoelectric strain coefficients (d_{33}) increased as the thickness of the porous layer and total porosity level of the layered structure increased. The permittivity (ε_{33}^{T}) decreased with increasing thickness and increasing porosity level of the porous layer due to the presence of a low permittivity air phase. These two factors in combination led to an increase in the longitudinal energy harvesting figure of merit, $d_{33}^2/\varepsilon_{33}^{T}$, for the layered structure, with a maximum of

3.74pm^2/N when the relative thickness of the porous layer was 0.52 and the porosity within this layer was ~60vol.%. This harvesting performance of these novel structures is much larger than both dense barium titanate (1.40pm^2/N) and barium titanate with randomly distributed porosity at the same 60% volume fraction (2.75pm^2/N).

1 Introduction

There is significant interest in the use of ferroelectric materials for energy harvesting applications due to their inherent ability to convert energy from mechanical vibrations and thermal fluctuations, via the piezoelectric and pyroelectric effects, respectively, to electrical energy. A variety of figures of merit (FOMs) have been devised to assist with the selection of piezoelectric materials for energy harvesting applications. When a piezoelectric is subjected to mechanical vibrations at low frequencies (<<100kHz) and away from the electromechanical resonance (i.e. off-resonance) the relevant FOM is given by [1]:

$$FOM_{ij} = {d_{ij}^2}\Big/{\varepsilon_{33}^T} \qquad (1)$$

where d_{ij} is the relevant piezoelectric strain coefficient associated with the direction of stress relative to the poling direction (such as d_{33} or d_{31}), ε_{33}^T is the permittivity at constant stress, T, and subscripts i and j follow conventional piezoelectric matrix notation. The FOM_{ij} is derived from capacitor energy storage equations ($E = \frac{1}{2}CV^2$, where E is stored electrical energy, C is capacitance and V is potential difference across a capacitor) and effectively describes the change in stored electrical energy within a piezo-active material when a stress is applied. Another important factor for effective piezoelectric energy conversion is the electromechanical coupling factor, k_{ij}^2, which takes into account the mechanical properties of the material and describes the efficiency of conversion from mechanical to electrical energy:

$$k_{ij}^2 = {d_{ij}^2}\Big/{\left(\varepsilon_{33}^T . S_{ij}^E\right)} \qquad (2)$$

where S_{ij}^E is the mechanical compliance at constant electric field. From Eqns. 1 and 2 it can be seen that optimum materials for energy harvesting mechanical loads should have high piezoelectric strain coefficients, low permittivity and low compliance.

One approach to reduce significantly the effective permittivity of piezoelectric composites is to introduce a low permittivity phase, such as air or a polymer ($\varepsilon_{33}^T \sim 1-10$), into the high permittivity ferroelectric ceramic; e.g. lead zirconate titanate (PZT, $\varepsilon_{33}^T \sim 1000-3500$, depending on composition) and barium titanate ($BaTiO_3$, $\varepsilon_{33}^T \sim 1500$) [2]. This has been achieved by introducing randomly distributed porosity throughout the ferroelectric microstructure [2] and has led to an increase in the longitudinal mode energy harvesting figure of merit, FOM_{33} [3], where $d_{ij} = d_{33}$ in Eqns. 1 and 2. The FOM_{33} increases as porosity is introduced into the material since there is a large reduction in permittivity and a relatively small decrease in d_{33}. By understanding the reasons behind the reduction in d_{33} and permittivity in porous ferroelectrics it is possible to design porous structures that yield further increases in the relevant FOMs, and will be discussed throughout this paper.

1.1 Poling of ferroelectrics

Ferroelectric ceramics, such as PZT and $BaTiO_3$, exhibit no bulk piezo- or pyro-electric properties when manufactured by traditional methods such as compaction of powders and heat-treatment at high temperature, known as sintering. This is due to the random distribution of domains as the polycrystalline material cools, post-sintering, below the Curie temperature and it relaxes to its lowest energy state, resulting in zero net polarisation [4]. To align the ferroelectric domains so as to yield the net polarisation required for ferroelectric ceramics to exhibit piezoelectric

behaviour the material has to be 'poled', whereby a large static electric field is applied across the material, usually at elevated temperatures close to the Curie point where the domains are more mobile. A ferroelectric material will become poled in the direction of the applied field, when the local electric field, E_f, (i.e. within a grain or domain) is greater than the coercive field, E_c, i.e. when $E_f > E_c$. In a dense single phase ferroelectric, E_f is homogenous, leading to a fully poled structure if the applied field is sufficiently large and greater than E_c. However, when a second phase with a different permittivity is introduced into the microstructure of the material the electric field will tend to concentrate in the low permittivity phase, in particular the pores of a porous ferroelectric material.

To illustrate this effect, the complex electric field distribution in a porous ferroelectric material is demonstrated in Fig. 1, which shows a two-dimensional finite element (FE) model of a single pore (relative permittivity, $\varepsilon_r = 1$) in barium titanate ($\varepsilon_r = 1500$) with a static electric field applied. This simulates the electric field distribution within a porous ferroelectric material during the poling process. A high electric field concentration (red contour in Fig. 1) is observed within the low permittivity pore while the field in the ceramic phase varies with location. Regions of low electric field (blue contour in Fig. 1) are observed in the immediate vicinity of the pore parallel to the direction of the applied field, which in a ferroelectric material may lead to incomplete poling in these regions. This phenomenon can be described by an adaptation of Gauss' law where the electric field, E_f, is related to the relative permittivity by the relationship [5]:

$$E_f = {}^{q}/_{(A.\,\varepsilon_r.\,\varepsilon_0)} \qquad (3)$$

where q is charge, A is area and ε_0 is the permittivity of free space. In a two phase material where $\varepsilon_1 \neq \varepsilon_2$ (subscripts denote phase), the electric field will not have the continuous and linear path that is present in a dense ferroelectric material during the poling procedure. As a consequence

of the field concentrating in the low permittivity air phase, porous ferroelectrics are difficult to pole, which reduces the effective piezoelectric response, and d_{ij}, of the material. Previous work has shown a gradual decrease in d_{33} as the porosity levels increase to 50-60vol.%. Beyond 60vol.% porosity there is a rapid decrease in d_{33} with increasing porosity [3, 6]. The decrease in d_{33} at high porosities is due to incomplete poling of the ferroelectric phase and cannot be counteracted by simply increasing the poling field, as high electric fields will eventually lead to electrical breakdown in either the air or in the ferroelectric ceramic.

A further consideration for designing porous ferroelectric ceramics is the increase in the elastic compliance, S_{33}^{E}, associated with the introduction of porosity, which is approximately proportional to the amount of porosity present for randomly distributed porosity [7]; the influence of spherical porosity on compliance of ceramics has been described in detail elsewhere [8, 9]. Therefore, despite the potential benefit of introducing porosity into ferroelectric ceramics for energy harvesting applications due to the significant reduction in permittivity, careful consideration of the porous structure is necessary to achieve improvements in harvesting FOMs and electromechanical coupling factors (see Eqn. 1 and 2).

One potential approach to improving both the mechanical and piezoelectric properties of porous piezoelectric composites is to consider porous piezoelectric 'sandwich layer' structures, where the porous layer is formed between two outer dense piezoelectric layers. A porous sandwich layer structure can be described in this case by two variables. Firstly, the relative thickness of the porous layer, which is defined as follows:

$$t_p^{rel} = thickness\ of\ porous\ layer/total\ thickness$$

$$= \frac{t_{porous}}{t_{porous}+2t_{dense}} \qquad (4)$$

based on the upper and lower dense layers being the same thickness, and secondly the porosity of the porous layer, discussed here in terms of volume percentage (vol.%). It should also be noted that in this paper, when comparing to previous work involving materials with uniformly distributed porosity [3], it is necessary to refer to the relative density, ρ_{rel}, of the overall ceramic structure. A relative density of unity is a ceramic with zero porosity (in reality pressureless sintered ceramics are typically $\rho_{rel} > 0.95$), such that the overall volume fraction of porosity, v_p, can be determined from $v_p = 1 - \rho_{rel}$.

2 Ferroelectric sandwich structures

The majority of previous research into porous sandwich structures and functionally graded porous ferroelectrics has focussed on the reduction in bulk permittivity leading to increased detection sensitivity for pyroelectric applications [11-14]. In this case the porosity (typically less than 16vol.% bulk porosity) acts to increase a variety of pyroelectric figures of merit, including the pyroelectric energy harvesting FOM_{pyro}, $F_E = p^2/\varepsilon_{33}^T$ [15], where p is the pyroelectric coefficient. The increase in FOM_{pyro} is due to a reduction in permittivity, although there is also a decrease in the pyroelectric coefficient as the level of porosity is increased. The significant reductions in permittivity are also of interest for piezoelectric energy harvesting, see Eqn. 1 and 2.

Work on piezoelectric sandwich layers of PZT for hydrophone applications also found that ε_{33}^T is reduced by the addition of a porous layer, which increases the voltage generated due to an acoustic pressure and the dense outer layers were found to improve the bending strength compared to PZT ceramics with uniformly distributed porosity [16]. Introducing graded porosity yielded enhanced acoustic matching, beneficial for hydrophone applications, as well as increasing the piezoelectric anisotropy leading to improved hydrostatic piezoelectric properties

[17, 18]. Compared to dense PZT, the addition of a porous inter-layer with ~25vol.% porosity led to a decrease in d_{33}, but it was significantly higher than a ceramic with the same volume fraction of uniformly distributed porosity [16].

The reported work on sandwich structures is experimental and no models have been presented that demonstrate an understanding of the impact of the complex electric field distribution, such as that shown in Fig. 1, in these structures during poling and the effect on the resulting piezoelectric properties. Such a study is necessary to understand the effect of a layered porous structure on both the energy harvesting FOM and the electromechanical coupling factor for harvesting and other transducer applications.

A variety of manufacturing methods have been used to create functionally graded and layered porous structures. Spin coating of $Pb_{0.8}La_{0.1}Ca_{0.1}Ti_{0.975}O_3$ [13] and deposition from a solution of $(Na_{0.85}K_{0.15})_{0.5}Bi_{0.5}TiO_3$ [14] has been used for producing thin films (≤500nm) of ferroelectric materials with enhanced pyroelectric FOMs. Tape casting has been used effectively to create PZT-based thick films (~1mm) with alternating dense and porous layers [11, 12, 16,] and porosity gradient materials [17]. Sequential compaction of individual layers provides a route to produce ferroelectric ceramic structures with thickness >1mm [18].

In this work barium titanate ceramics with porous sandwich layer structures have been evaluated both numerically and experimentally for their energy harvesting capabilities, with particular attention paid to the effect of the relative thickness of the porous inter-layer and the porosity level of the inter-layer on the relevant properties and performance figures of merit. The properties of these structures are compared to that of dense and uniformly distributed porous barium titanate used to create the layers. Barium titanate was used in this investigation rather than PZT so as to enable comparison to previous data [3].

3 Finite element modelling

3.1 Models of porous ferroelectric ceramics

A variety of models exist that were designed to evaluate the effect of introducing a low permittivity second phase (such as air or a polymer) into ferroelectric ceramics (usually PZT) on the piezoelectric and dielectric properties [19-30]. A common assumption in such models, often based on the 'unit cell' approach, is that the ferroelectric material is *fully poled,* irrespective of the porosity levels. This is a simplification that leads to a disagreement between the models and experimental data, as highlighted by Fig. 1 where we see a complex field distribution in the high permittivity phase due to the presence of a pore can result in a partially poled material, and therefore lower effective piezoelectric properties of a porous ferroelectric ceramic. A more accurate approach for modelling porous piezoelectric ceramics was found using a finite element model that accounted for this complex electric field distribution within a porous ferroelectric during the poling process [6].

In this paper the approach proposed by Lewis et al. [6] has been further developed to investigate how the addition of a porous layer between two dense layers to form a sandwich structure affects the poling behaviour of these materials. By developing a detailed understanding of how the effective longitudinal piezoelectric response, d_{33}, and permittivity changes with the porous layer thickness and the level of porosity after the poling process, it is possible to design porous structures with significantly improved properties for energy harvesting applications.

3.2 Modelling methodology

A finite element (FE) approach has been used whereby a three dimensional cubic mesh with 27,000 elements (30 x 30 x 30) was arranged into dense outer layers and a porous inter-layer, see Fig. 2. Models were created where varying levels of inter-layer porosity were achieved by

changing the ratio of cells randomly assigned with the properties of either unpoled $BaTiO_3$ ceramic [31] or air; the outer layers were assumed to be fully dense (i.e. no pores). The $BaTiO_3$ elements in the model can be thought of as representing multi-grain, and therefore multi-domain, regions that have no net polarisation when the geometry is initially generated so as to simulate the properties of sintered, unpoled ferroelectric ceramics prior to poling. The relative porous layer thickness, t_p^{rel}, defined in Eqn. 4, was varied from $0 \leq t_p^{rel} \leq 1$, such that when $t_p^{rel} = 0$ the structure is fully dense and when $t_p^{rel} = 1$ the structure has uniformly distributed porosity with no dense layers. The increment at which t_p^{rel} was varied was as close to 0.1 as possible, whilst maintaining the sandwich layer in the middle of the structure, meaning that at certain values the step was displaced by $^1/_{30}$, i.e. 0.1 became 0.13.

Once the network of cells used to create the sandwich structure had been generated, electrodes were simulated by coupling the voltage degrees of freedom at the upper and lower faces of the three-dimensional model. An electric field (0.6MV/m) that was higher than the coercive field (E_c = 0.5MV/m [32]) was applied between the electrodes to simulate the poling procedure and the local electric field analysed in each element. The poling electric field was selected as it gave a good fit to the experimental data for $BaTiO_3$ with uniformly distributed porosity, from [3], using the porous network model detailed in [6]. The use of higher poling fields leading to an overestimation of effective piezoelectric properties at high porosities, see supplementary information Fig. S1. Elements in which the local field in the z-direction, E_f^z, was greater than the coercive field, E_c, of $BaTiO_3$ became 'poled' in this direction. Early versions of the porous network model allowed poling of elements in six possible directions (*-x*, *x*, *-y*, *y*, *-z* and *z*) [6], analogous to the six tetragonal poling directions in a unit cell of $BaTiO_3$ [33], however, it was found that the effect of elements poled in directions other than the z-direction on the effective d_{33} was negligible (a maximum of 1.5% of the elements poled in the z-direction for any given geometry) and so the

model was simplified to only pole elements in the z-direction. Input data of compliance, permittivity and piezoelectric properties for the coupled-field FE model is contained in Table 1 poled material [34] and an E_c value of 0.5MV/m was used [32]. The permittivity of the unpoled $BaTiO_3$ (ε_r = 1187.5) is an average of the constant strain permittivity of poled $BaTiO_3$ in the 1- and 3-directions. After establishing the distribution of material poled in the z-direction a potential difference, V, was applied between the electrodes of the poled model and the resulting strain used to calculate the effective piezoelectric strain coefficient, d_{33}. The effective permittivity was calculated from the charge (Q) developed at the electrodes and using the relationship $Q = CV$, where C is capacitance.

3.3 Modelling results

Figs. 3 to 5 show the modelled data for the piezoelectric d_{33} coefficient, permittivity (ε_{33}^T) and FOM_{33} as a function of porous layer relative thickness (t_p^{rel}). The data is averaged from 30 runs at each t_p^{rel} and layer porosity and is shown for the porosity level of 10-60vol.% in the centre porous layer. Layer porosities of greater than 60vol.% could not be investigated as this led to a high fraction of 'floating' $BaTiO_3$ elements, i.e. those surrounded completely by air. These high porosity fractions are also difficult to manufacture (as discussed in the experimental section).

Fig. 3 shows that at low inter-layer porosity levels (≤20vol.%) there is no significant variation in d_{33} across the full range of t_p^{rel}. However, as the porosity is increased to 30vol.% and 40vol.% a large decrease in d_{33} is observed as the porous layer relative thickness (t_p^{rel}) is gradually increased from zero. Past the local minima an increase in d_{33} is then observed with increasing t_p^{rel}. For sandwich layer structures with high porosity inter-layers (50 and 60 vol.%) the d_{33} initially falls steeply as t_p^{rel} is gradually increased, before subsequently rising with further increases in t_p^{rel} and eventually reaching a local maxima of d_{33} before declining as t_p^{rel} is further

increased toward unity, where we have a uniformly distributed porous $BaTiO_3$. The model prediction of effective d_{33} of the multi-layered structure is intrinsically linked to the fraction of material poled, which can be seen in Fig. 6 where both d_{33} and fraction of $BaTiO_3$ poled in the z-direction are plotted as a function of porous layer thickness and for different layer porosities. The paths followed by both curves are very similar with maximum points occurring at the same relative thickness for all layer porosities. The effective d_{33} appears to be dependent on other factors as well as the fraction of poled material, such as its distribution throughout the structure, but the trend is quite clear when porosity is uniformly distributed throughout the structure, which is shown in supplementary Fig. S2. The physical origin of the turning points on the plot discussed in detail later.

The relative permittivity gradually decreases as the relative porous layer thickness increases and the fraction of low permittivity porosity in the inner layer increases, see Fig. 4. The model indicates that the relative permittivity of the overall structure is primarily a function of the amount of high permittivity $BaTiO_3$ material, i.e. the overall relative density, and is not significantly affected by the amount of material poled.

The predicted d_{33} and ε_{33}^T from the model were then used to calculate FOM_{33} using Eqn. 1 and results are shown in Fig. 5. In all cases, the uniformly distributed porosity material (i.e. $t_p^{rel} = 1$) has a higher FOM_{33} than the dense material (i.e. $t_p^{rel} = 0$); the value for the dense material is 1.53pm^2/N. The layered structure at 60% porosity and $t_p^{rel} = 0.73$ has a FOM_{33} of 2.23pm^2/N, which is higher than the value of 1.91pm^2/N for the uniformly distributed porous material at $t_p^{rel} = 1$. This is a result of high d_{33} (Fig. 3) and low permittivity (Fig. 4). The high FOM_{33} indicates the potential of porous sandwich layer structures for piezoelectric energy harvesting applications.

3.4 Discussion

The unusual dependence of the d_{33} and FOM_{33} on relative porous layer thickness (Fig. 3 and Fig. 5) is a result of the complex poling behaviour of the structures at high layer porosities (≥30vol.%), resulting in incomplete poling of the structure, (see also in Fig. 6). This can be better understood by analysing the local electric field in each phase ($BaTiO_3$ or air) in the FE model in both the dense and porous layers. Histograms of the electric field in $BaTiO_3$ z-direction (i.e. poling axis) during the poling process of the model at 0.6MV/m are shown in Fig. 7 for a structure with a layer porosity of 60vol.% and relative thickness (t_p^{rel}) values of 0.2, 0.6 and 0.93 (top, middle and bottom images of Fig. 7, respectively). Images of poled material distributions for corresponding sample geometries and porosity are shown in the histograms with blue regions representing unpoled $BaTiO_3$ elements and red regions are elements poled in the z-direction. A sandwich layer porosity of 60vol.% was selected to demonstrate how the distribution of poled material changes with porous layer thickness shown in the histograms as the model predicts it has the greatest FOM_{33}; see Fig. 5. The dashed line at 0.5MV/m indicates the coercive field, E_c: all $BaTiO_3$ elements subjected to fields greater than this value are poled in the z-direction, and contribute to the resulting piezoelectric d_{33} coefficient.

For a low thickness porous layer ($t_p^{rel} = 0.2$), ~80% of $BaTiO_3$ elements in the dense layers have a local z-field of $0.4 < E_f < 0.45$ MV/m, indicating a relatively homogenous field distribution but one that lies below the coercive field so that the $BaTiO_3$ in this layer remains largely unpoled, see the upper histogram and the poling distribution in the inset of Fig. 7. However, high field concentrations in the thin porous layer for both the $BaTiO_3$ and air phase are observed, but as the total number of polarizable elements in this thin region is low, the total volume fraction poled and d_{33} is low, see Fig. 6. When $t_p^{rel} = 0.6$ (middle histogram and poling distribution inset, Fig. 7) the electric field in the dense layer remains relatively homogenous, however there is a shift

towards lower field strengths compared to $t_p^{rel} = 0.2$ so there is almost no poling of the dense $BaTiO_3$ layers. Once again the electric field concentrates in the central porous layer of lower permittivity, with the highest fields in the air phase. A more homogenous distribution of field in the porous layer is observed for $t_p^{rel} = 0.6$ compared to $t_p^{rel} = 0.2$ and over 50% of elements in this central layer are greater than the coercive field and are poled, leading to the increase in d_{33} for a layer porosity of 60vol.% from $0.2 < t_p^{rel} < 0.6$, as seen in Fig. 6.

As the layer porosity is further increased to $t_p^{rel} = 0.93$ (lower histogram and poling distribution inset, Fig. 7) the field strengths in the dense layers shift to even lower magnitudes, such that no material is poled in the thin outer dense layers. This can be explained by examination of Fig. 1, whereby the regions above and below a low permittivity region (i.e. the pore in Fig. 1 or the porous layer in the layered structure) and parallel to the applied field are subject to the lowest electric fields and are not poled in the direction of the field. The field in the porous layer in both the $BaTiO_3$ and the air is the most homogenous for this thick porous layer, however, due to a the shift to lower field strengths, less than 25% of the $BaTiO_3$ volume in the porous layer is subjected to fields above E_c. As a result, the d_{33} decreases for $t_p^{rel} = 0.93$ compared to $t_p^{rel} = 0.6$.

These results indicate that the presence of a thin porous layer with high porosity leads to high field concentrations in both the $BaTiO_3$ and air in the porous layer, compared to when the porous layer is relatively thick. As a result of Gauss' Law (Eqn. 3), the electric field increasingly concentrates in the porous layer as the ratio between the effective permittivity of the dense and porous layers increases, i.e. as the porosity in the central layer increases. When the porosity in the inner layer is large (≥ 30vol.%), the high fields in the porous region for thin porous layers (i.e. low t_p^{rel}) result in a high fraction of ceramic in the porous layer becoming poled. However the volume of $BaTiO_3$ in the porous layer is low relative to the total volume material, hence there

is a rapid decrease in d_{33} (Fig. 3, *points 1→2*). As the porous layer thickness and volume is increased, the electric field strengths in this layer decrease but are still sufficiently large to pole a high fraction of $BaTiO_3$ in this region, leading to an increase in d_{33} (Fig. 3, *points 2→3*). This phenomenon is only observed when the layer porosity is ≥30vol.% so that there is a large difference between the effective permittivity of the dense and porous layers. When the porosity of the central layer is low (10 and 20vol.%) the ratio of the permittivity of the dense and porous layers is also low, and while the electric field continues to concentrate in the porous layer the decrease in field in the dense layers is not sufficiently large to fall below the coercive field, E_c, so that most of the $BaTiO_3$ elements are poled, contributing to the high d_{33} values observed from $0 \leq t_p^{rel} \leq 1$ (see Fig. 6). At very high layer porosities (≥50vol.%) a peak value for d_{33} is observed before a decrease with further increases in t_p^{rel} as there is no longer a sufficient field concentration in the porous layer to pole a significant fraction of the $BaTiO_3$ material, thus leading to a decrease in d_{33} (Fig. 3, *points 3→4*).

4 Experimental

4.1 Fabrication of $BaTiO_3$ with porous sandwich layer

Sandwich layer structures were manufactured to compare with the modelling outputs. In order to fabricate the dense outer layers the starting powder was produced by ball milling barium titanate powder (*Ferro,* UK) with 5wt.% binder, polyethylene glycol (PEG) (*Sigma,* UK) in distilled water for 24 hours before drying and regrinding. To form the inner porous layer the burned out polymer spheres (BURPS) process was used, with the starting powder produced by dry-mixing the barium titanate powder with varying proportions of PEG (25 and 35wt.%) to enable the production of layered structures with different sandwich layer porosities. Green barium titanate pellets (13mm diameter) were formed by alternately adding dense and porous

starting powder into the uniaxial pellet die, gently flattening the powder between each layer and pressing at 185MPa. The ratio of the amount of dense and porous starting powder was varied to produce layers of different relative thicknesses whilst attempting to achieve similar final pellet dimensions. Pressureless sintering of the green ceramics was conducted in air at 1300°C for two hours, which included a two hour dwell stage on the up-ramp at 400°C to burn off the PEG pore forming agent. The ramp rate throughout the sintering process was ±60°C/h. Post sintering, samples were ground flat and cleaned, silver electrodes were applied (*RS Components, Product No 186-3600*) and the layered structures were then subjected to corona poling in air at 115°C with a 14kV field applied from a 35mm point source. These processing conditions are similar to those detailed in [3] to allow comparison between fully dense, fully porous (uniform distribution of porosity) and the porous sandwich layer barium titanate, as in Fig. 2. Using >20wt.% of PEG was found to reduce cracking during the pressing stage, such that producing samples with a lower inter-layer porosity was not achievable using the fabrication methods used in this investigation. Other methods, such as tape casting have previously demonstrated the potential for forming layered structures with inter-layer porosities of less than 30vol.% [11, 12, 16]. Very high levels of porosity (>60vol.%) cause a significant reduction in mechanical properties and so were not investigated.

Piezoelectric strain coefficients, d_{33} and d_{31}, were measured using a *Take Control Piezometer PM25* system. The dielectric properties of the material were measured via impedance spectroscopy using a *Solartron 1260* and *1296 Dielectric Interface* over a frequency range of 1Hz to 1MHz, and reported in this paper at 1kHz. Optical and scanning electron microscopy (SEM) were used to investigate the bulk laminate structure and the porous microstructure. The relative density and apparent porosity of the samples was measured using the Archimedean method.

The porous layer relative thickness, t_p^{rel}, was estimated from the average relative density measured of the dense layers (ρ_{rel} = 0.93) and the average relative densities of the porous layer as a result of the amount of pore former used in the starting powder from previous work [3]: ρ_{rel} = 0.40 for 35wt.% PEG and ρ_{rel} = 0.50 for 25wt.% PEG. This was compared to measurements taken from SEM images using ImageJ software and found to be a satisfactory estimate.

4.2 Structural characterisation of layered materials

After sintering, the relative density of the dense layers was found to be 0.93, slightly lower than the density achieved in the uniform dense material (ρ_{rel} = 0.95 [3]). This was likely to be due to the lower pressing force required to produce crack-free sandwich layered samples. SEM images of two sandwich-layered structures with two different thicknesses are shown in Fig. 8 (t_p^{rel} of ~0.25 and ~0.48). All samples were polycrystalline with grain sizes in the range of 10 - 30μm; the microstructure from a dense layer with ρ_{rel} = 0.93 is shown as an inset to Fig. 8a. Despite lowering the pressing force some small cracks could be observed between layers perpendicular to the pressing direction in Fig. 8b, which are thought to form during sintering, where differences in shrinkage between the porous and dense layers can cause thermal stresses. An additional difficulty encountered during the preparation of samples was achieving layers exactly perpendicular to the pressing direction that may have had an effect on the repeatability of results; a porous sandwich layer with a small slanted orientation with respect to the parallel outer dense surfaces of the layered $BaTiO_3$ can be seen in Fig. 8b.

4.3 Piezoelectric strain coefficients, d_{33} and d_{31}

The measured longitudinal piezoelectric strain coefficient, d_{33}, exhibited a similar trend as predicted by the FE model and is shown in Fig. 9, as a function of both relative density (bottom x-axis) and porous layer relative thickness, t_p^{rel} (top x-axes with colours relevant to the data

sets), for both 50 and 60vol.% layer porosity for a poling voltage of 0.6MV/m in the model. A comparison of the effect of using higher poling fields in the model (0.7 and 0.8MV/m) for these sample conditions is shown in the supplementary information, Fig. S3, indicating that higher effective d_{33} values (i.e. more complete poling) may be achievable if it were possible to experimentally pole porous samples at larger electric fields. However, dielectric breakdown occurs at lower field strengths than for dense samples due to field concentrations around the pores, which is a practical limitation of processing these materials. The experimental data was found to be higher than in the model, which is thought to be due to differences in the applied fields between the model and during corona poling of the manufactured samples (i.e. the experimental samples exhibited a higher degree of poling than was observed in the model). Both experimental data and the model indicate the porosity of the sandwich layer was not found to have a significant influence on the d_{33} coefficients in the t_p^{rel} region studied, with maximum experimental values of >120pC/N measured in structures with different porosity sandwich layers and overall relative density of ~0.70, values which are comparable to that of dense $BaTiO_3$ [3] (average d_{33} = 124.8pC/N). These values are higher than d_{33} observed in uniformly distributed porous $BaTiO_3$ with similar levels of porosity as the inner layer (average of 86.8pC/N for 60vol.% porosity and 99.5pC/N for 50vol.% porosity [3]) and overall porosity of 32vol.%, i.e. ρ_{rel} = 0.68 (average d_{33} = 102.4pC/N).

The transverse piezoelectric coefficient, d_{31}, shown in supplementary information Fig. S4, also reduces with increasing layer thickness, and coupled with high d_{33}, values would lead to significantly improved hydrostatic piezoelectric coefficient, $d_h = d_{33} + 2d_{31}$; this may make layered porous structures of interest for use in other applications such as hydrostatic sensors (high d_h or g_h). It is of interest to note that the low d_{31} of the porous sandwich layers structures

manufactured in this work make them unsuitable for 31-mode mode energy harvesters *(FOM_{31})*, such as cantilevers, where high d_{31} coefficients are necessary, see Eqn. 1 and 2.

4.4 Permittivity and FOM_{33}

The permittivity of porous sandwich layer structures reduced with increasing porous layer relative thickness and with an increase in the porosity level of the layer. This is shown in Fig. 10 as a function of relative density (bottom x-axis) and porous layer relative thickness (top x-axes with colours relevant to the data sets). The FE model (solid line in Fig. 10) provides a good fit the experimental data (points), particularly when $\rho_{rel} < 0.75$. Concentrating the porosity in a sandwich layer, rather than being uniformly distributed, was found to be beneficial in terms of reducing permittivity as can be seen by comparing the fit of the experimental data for uniformly porous $BaTiO_3$ (dashed black line), from [3], to the sandwich layer materials in Fig. 10. This may also be beneficial in terms of elastic compliance, S_{33}^E, as lower permittivities are observed in sandwich structures for the same overall volume of porosity than in uniform porous materials; further work is necessary to characterise any potential improvement in terms of compliance and the resulting effect on electromechanical coupling coefficient, k_{33}^2, see Eqn. 2. The findings presented here indicate that tuning of the permittivity is possible by careful positioning of the porosity within the inner layer of the structure.

The longitudinal energy harvesting figure of merit, FOM_{33}, was calculated from the experimental d_{33} and ε_{33}^T data using Eqn. 1, and is shown in Fig. 11 as a function of relative density, alongside data obtained for porous $BaTiO_3$ with uniformly distributed porosity that is reported elsewhere [3]. The combined effect of high d_{33} values that are comparable to that of dense $BaTiO_3$ (Fig. 9) and significant reductions in permittivity compared to both dense and uniform porous $BaTiO_3$ (Fig. 9) resulted in a maximum FOM_{33} = 3.74pm^2/N (layer porosity ~60vol.%, t_p^{rel} = 0.52), which

is a factor of 2.65 higher than the value for dense $BaTiO_3$ (FOM_{33} = 1.40 pm^2/N) and 1.3 times higher than highest FOM_{33} for porous $BaTiO_3$ with uniformly distributed porosity (FOM_{33} = 2.85pm^2/N and ~60vol.% porosity), see Fig. 11. Data for the measured d_{33}, ε_{33}^{T} and FOM_{33} is summarised in Table 2 for dense $BaTiO_3$, $BaTiO_3$ with uniformly distributed porosity and the layered structures manufactured for this work. The increase in FOM_{33} demonstrates the potential for ferroelectric porous sandwich layer structures for applications such as energy harvesting.

5 Conclusions

This paper describes the modelling, fabrication and characterisation of novel layered barium titanate ceramics that have been produced with dense outer layers and a porous 'sandwich' layer. Properties have been evaluated both numerically and experimentally for their energy harvesting capabilities and compared to both dense $BaTiO_3$ and $BaTiO_3$ with uniformly distributed porosity. It was found that d_{33} values increased with porous layer relative thickness in materials with high porosity layers, a counterintuitive phenomenon that has not been observed previously.

Finite element modelling was used to demonstrate that the increase in d_{33} with porous layer thickness, observed at high internal layer porosities (≥30vol.%), was due to complexities in the poling of these ferroelectric materials that caused them become only partially poled in the direction of the applied poling field. This effect was more pronounced in structures with a high porosity sandwich layer due to large differences in effective permittivity between dense and porous layers causing high field concentrations in the porous layer. The amount of polarisable material in the porous layer was found to be important with regard to measured piezoelectric properties in materials with high inter-layer porosities, such that increases in d_{33} were observed

with increasing porous layer thickness, i.e. *increased* levels of porosity. This resulted in a predicted optimum layer porosity (60vol.%) and relative thickness ($t_p^{rel} = 0.73$) to maximise the modelled energy harvesting figure of merit. Good agreement with experimental data was observed that could not have been predicted using a model that assumes the material is fully poled. The modelling approach developed in this paper has shown the importance of considering the complex distribution of poled material that is likely to occur when manufacturing and poling porous ferroelectric materials.

High longitudinal piezoelectric d_{33} coefficients, comparable to those measured in dense $BaTiO_3$ (~120pC/N), were observed experimentally in porous sandwich layer structures using high porosity (≥50vol.%) layers with a high porous layer thickness ($t_p^{rel} = 0.52$). The high d_{33}, coupled with the low permittivity, leads to high longitudinal energy harvesting figures of merit, FOM_{33}, that were found to improve on harvesting figures of merits measured in both dense and uniform porous $BaTiO_3$ by factors of 2.65 and 1.30, respectively. These significant improvements demonstrate the potential of porous sandwich layer ferroelectric ceramics to design high performance materials for energy harvesting and sensing applications.

Acknowledgements

J. I. Roscow would like to acknowledge EPSRC for providing financial support during this research. C. R. Bowen would like to acknowledge funding from the European Research Council under the European Union's Seventh Framework Programme (FP/2007-2013)/ERC Grant Agreement no. 320963 on Novel Energy Materials, Engineering Science and Integrated Systems (NEMESIS).

References

[1] R.A. Islam, S. Priya, Realization of high-energy density polycrystalline piezoelectric ceramics, J. App. Phys. Lett. 88 (2006) 032903.
[2] R.E. Newnham, D.P. Skinner, L.E. Cross, Connectivity and piezoelectric-pyroelectric composites, Mater. Res. Bull. 13 (1978) 525-536.
[3] J.I. Roscow, J. Taylor, C.R. Bowen, Manufacture and characterization of porous ferroelectrics for piezoelectric energy harvesting applications, Ferroelectrics 498 (2016) 40-46.
[4] G. Haertling, Ferroelectric Ceramics: History and Technology. J. Am. Ceram. Soc. 82 (1999) 797–818.
[5] I.S. Grant, W.R. Phillips (1990). Electromagnetics, second ed., Wiley.
[6] R.W.C. Lewis, A.C.E Dent, R. Stevens, C.R. Bowen, Microstructural modelling of the polarization and properties of porous ferroelectrics, Smart Mater. Struct. 20 (2011) 085002.
[7] T. Zeng, X. Dong, S. Chen, H. Yang, Processing and piezoelectric properties of porous PZT ceramics, Ceram. Inter. 33 (2007) 395-399.
[8] R.W. Rice, Evaluation and extension of physical property-porosity models based on minimum solid area, J. Mater. Sci. 31 (1996) 102-18.
[9] A.P. Roberts, E.J. Garboczi, Elastic properties of model porous ceramics, J. Am. Ceram. Soc. 83 (2000) 3041-8.
[10] C.R. Bowen, A. Perry, A.C.F. Lewis, H. Kara, Processing and properties of porous piezoelectric materials with high hydrostatic figures of merit. J. Eur. Ceram. Soc. 24 (2004) 541–545.
[11] A. Navarro, R.W. Whatmore, J.R. Alcock, Preparation of functionally graded PZT ceramics using tape casting, J. Electroceram. 13 (2004) 413–415.
[12] C.P. Shaw, R.W. Whatmore, J.R. Alcock, Porous, functionally gradient pyroelectric materials, J. Am. Ceram. Soc. 90 (2007) 137-142.
[13] Q.G. Chi, W.L. Li, W.D. Fei, Y. Zhao, Enhanced performance of sandwich structure $Pb_{0.8}La_{0.1}Ca_{0.1}Ti_{0.975}O_3$ thins films for pyroelectric applications, Mater. Lett. 63 (2009) 1712-1714.
[14] Q.G. Chi, J. Dong, J, C. Zhang, X. Wang, Q. Lei, (2016). Highly (100)-oriented sandwich structure of $(Na_{0.85}K_{0.15})_{0.5}Bi_{0.5}TiO_3$ composite films with outstanding pyroelectric properties, J. Mater. Chem. C 4 (2016) 4442–4450.
[15] C.R. Bowen, J. Taylor, E. Le Boulbar, D. Zabek, V.Yu. Topolov, A modified figure of merit for pyroelectric energy harvesting, Mater. Lett. 138 (2015) 243-246.

[16] L. Palmqvist, K. Palmqvist, C.P. Shaw, Porous multilayer PZT materials made by aqueous tape casting, Key Eng. Mater. 333 (2007) 215-218.
[17] E. Mercadelli, A. Sanson, P. Pinasco, E. Roncari, C. Galassi, Tape cast porosity-graded piezoelectric ceramics, J. Eur. Ceram. Soc. 30 (2010) 1461-1467.
[18] D. Piazza, C. Capiani, C. Galassi, Piezoceramic material with anisotropic graded porosity, J. Eur. Ceram. Soc. 25 (2005) 3075-3078.
[19] H.R. Gallantree, Piezoelectric ceramic/polymer composites, British Ceram. Proc. 41 (1989) 161-169.
[20] H. Banno, Effects of porosity on dielectric, elastic and electromechanical properties of $Pb(Zr,Ti)O_3$ ceramics with open pores: a theoretical approach, Jpn. J. App. Phys. 32 (1993) 4214-4217.
[21] M.L. Dunn, M. Taya, Electromechanical properties of porous piezoelectric ceramics, J. Am. Ceram. Soc., 79 (1993) 1697-1706.
[22] C.R. Bowen, H. Kara, Pore anisotropy in 3-3 piezoelectric composites, Mater. Chem. Phys. 75 (2002) 45-49.
[23] F. Levassort, M. Lethiecq, R. Desmare, L.P. Tran-Huu-Hue, Effective electroelastic moduli of 3-3(0-3) piezocomposites, IEEE Trans. Ultrason., Ferroelect., Freq. Control, 46 (1999) 1028-1034).
[24] C.R. Bowen, V.Yu. Topolov, Piezoelectric sensitivity of $PbTiO_3$-based ceramic/polymer composites with 0-3 and 3-3 connectivity, Acta Mater. 51 (2003) 4965-4976.
[25] R. Ramesh, H. Kara, C.R. Bowen, Finite element modelling of dense and porous piezoceramic disc hydrophones, Ultrason. 43 (2005) 173-181.
[26] R. Kar-Gupta, T.A. Venkatesh, Electromechanical response of porous piezoelectric materials: Effects of porosity distribution, App. Phys. Lett. 91 (2007) 062904.
[27] S. Iyer, T.A. Venkatesh, Electromechanical response of porous piezoelectric materials: Effects of porosity connectivity, App. Phys. Lett. 97 (2010) 072904.
[28] K.S. Challagulla, T.A. Venkatesh, Electromechanical response of piezoelectric foams, Acta Mater. 60 (2012) 2111-27.
[29] P.W. Bosse, K.S. Challagulla, T.A. Venkatesh, Effects of foam shape and porosity aspect ratio on the electromechanical properties of 3-3 piezoelectric foams. Acta Mater. 60 (2012) 6464-75.
[30] S. Iyer, M. Alkhader, T.A Venkatesh, Electromechanical response of piezoelectric honeycomb foam structures, J. Am. Ceram. Soc. 97 (2014) 826-34.

[31] A.C. Dent, C.R. Bowen, R. Stevens, M.G. Cain, M. Stewart, Effective elastic properties for unpoled barium titanate, J. Eur. Ceram. Soc. 27 (2007) 3739-43.
[32] D.A. Berlincourt, H.A. Krueger, C. Near, Properties of Morgan electro ceramic ceramics, Technical Publication TP-226 (1999) 1–12.
[33] G. Kwei, A. Lawson, Structures of the ferroelectric phases of barium titanate, J. Phys. Chem. 97 (1993) 2368–77.
[34] D.A. Berlincourt, D.R. Curran, H. Jaffe, Physical acoustics. Principles and methods. Vol 1. Methods and devices. Pt A., New York: Academic Press, 1964, p. 169.

Tables

Table 1: Material input data of poled $BaTiO_3$ where c_{ij}^E is the stiffness matrix (GPa), e_{ij} is used to define the piezoelectric coefficient matrix (C/m^2) and $\varepsilon_{ij}^S/\varepsilon_0$ is the relative permittivity at constant strain.

C_{11}^E	C_{12}^E	C_{13}^E	C_{33}^E	C_{44}^E	e_{31}	e_{33}	e_{15}	$\varepsilon_{11}^S/\varepsilon_0$	$\varepsilon_{33}^S/\varepsilon_0$
150.0	66.0	60.0	146.0	44.0	-4.35	17.5	11.4	1115	1260

Table 2: Comparison of average and max longitudinal piezoelectric coefficients (d_{33}), relative permittivity ($\varepsilon_{33}^T/\varepsilon_0$) and energy harvesting figure of merits (FOM_{33}) for dense, uniformly distributed porous (from previous investigation [3]) and selected layered porous barium titanate.

Sample type	Average relative density (%)	Sandwich layer relative thickness	Sandwich layer porosity (vol.%)	Average d_{33} (pC/N)	Max d_{33} (pC/N)	Average $\boldsymbol{\varepsilon_{33}^T/\varepsilon_0}$	Average FOM_{33} (pm^2/N)
Dense	94.9	-	-	124.8	144.5	1527	1.31
Uniform porosity	88.8	-	-	95.8	107.5	1362	0.76
	80.7	-	-	91.8	99.5	1170	0.81
	68.0	-	-	102.4	106.0	794	1.49
	62.4	-	-	98.0	109.0	759	1.43
	50.2	-	-	99.2	113.0	528	2.11
	39.2	-	-	88.9	99.0	377	2.37
	34.0	-	-	61.3	74.5	284	1.49
	27.7	-	-	42.5	48.0	167	1.22
Sandwich	86.0	0.15	60	92.0	96.0	1040	0.92
	81.5	0.23	60	104.7	110.0	826	1.50
	72.5	0.40	60	114.9	122.0	583	2.56
	66.0	0.52	60	119.3	124.5	484	3.34
	84.1	0.22	50	104	104.0	1049	1.16
	78.1	0.36	50	99.5	106.5	801	1.41
	73.5	0.46	50	118.1	123.5	732	2.15

Figures

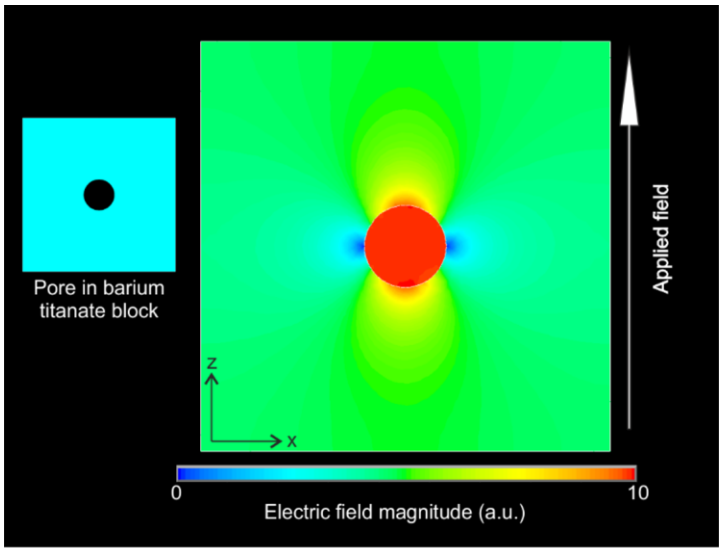

Figure 1: *Contour plot of local electric field magnitude (arbitrary units) due to an applied field across a two dimensional finite element model whereby a circular pore of low permittivity is contained within a high permittivity barium titanate matrix. Blue regions represent areas of low field in the $BaTiO_3$ phase that may result incomplete poling in a porous ferroelectric material.*

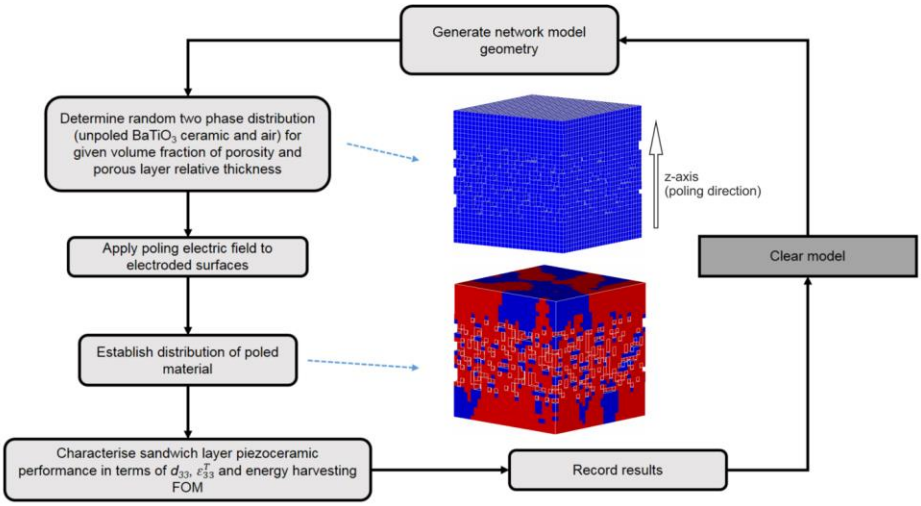

Figure 2: *Flow diagram of finite element modelling process using Ansys APDL. The upper image in the centre of the diagram shows the network geometry of unpoled $BaTiO_3$ ceramic (blue regions) and pores in the layer 'sandwiched' between two outer dense layers. The lower image shows the poled geometry where red regions represent poled $BaTiO_3$ and blue regions remain unpoled.*

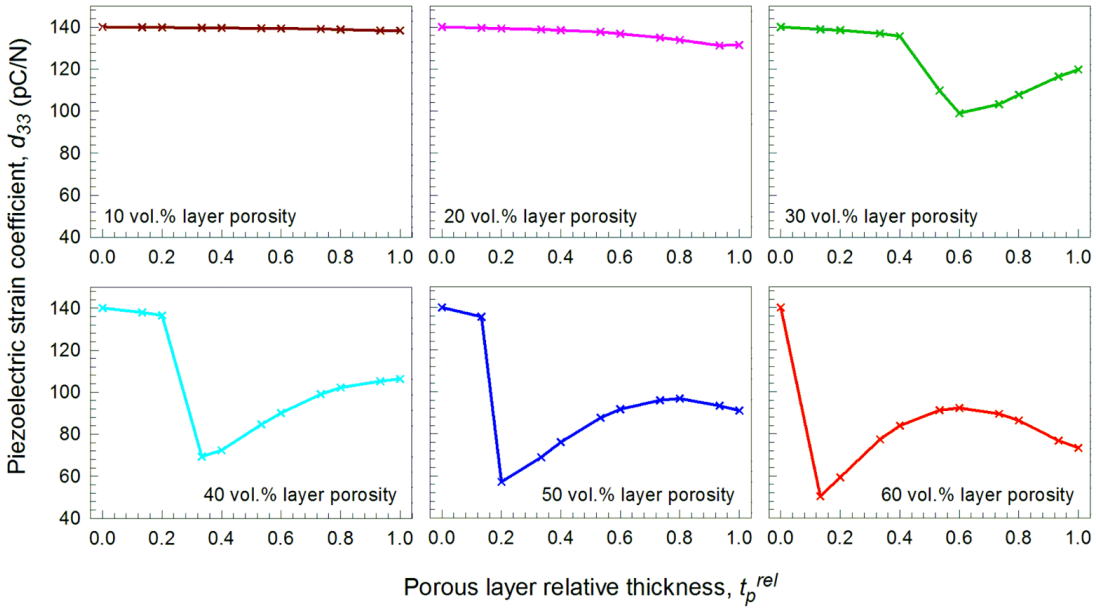

Figure 3: *Finite element model data showing the effect of porous layer relative thickness and inter-layer porosity on longitudinal piezoelectric strain coefficient, d_{33}.*

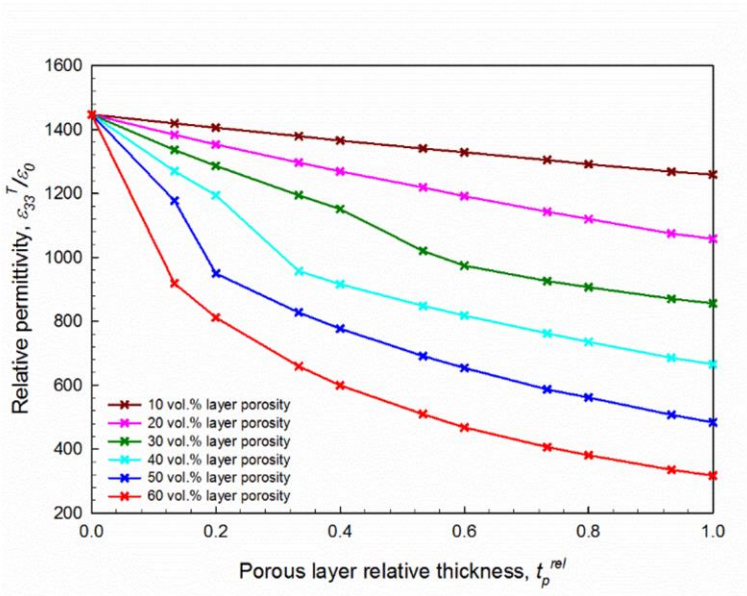

Figure 4: *Finite element model data showing the effect of porous layer relative thickness and layer porosity on relative permittivity, which decreases with increasing porosity in all cases, i.e. both as layer thickness and layer porosity are increased.*

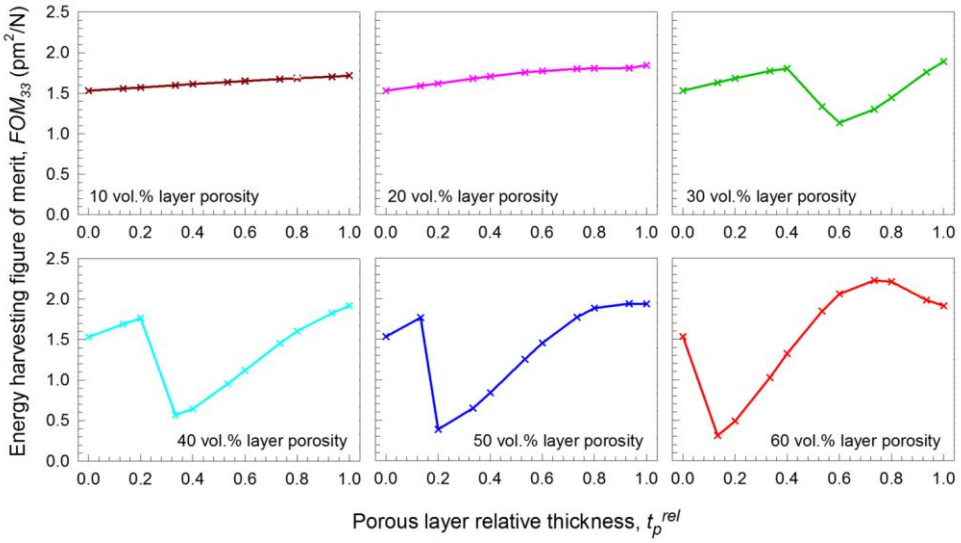

Figure 5: *Finite element model data showing the effect of porous layer relative thickness and porosity level of layer on longitudinal energy harvesting figure of merit, FOM_{33} ($d_{33}^2/\varepsilon_{33}^T$).*

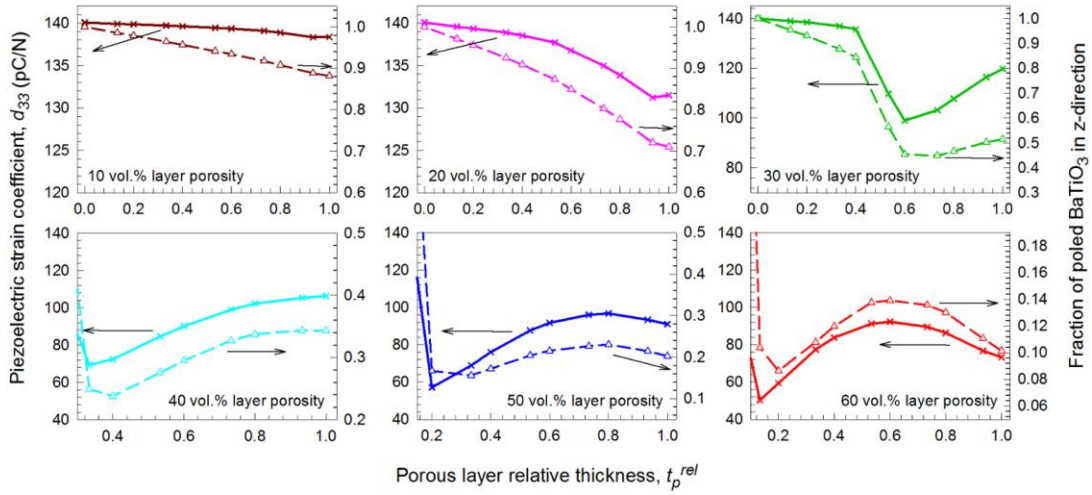

Figure 6: Finite element model data of effect of sandwich layer relative thickness and porosity on the d_{33} (left axes, solid lines) and fraction of poled $BaTiO_3$ in z-direction (right axes, dashed lines), demonstrating the link between the fraction of material poled in the z-direction and the effective piezoelectric properties of the material.

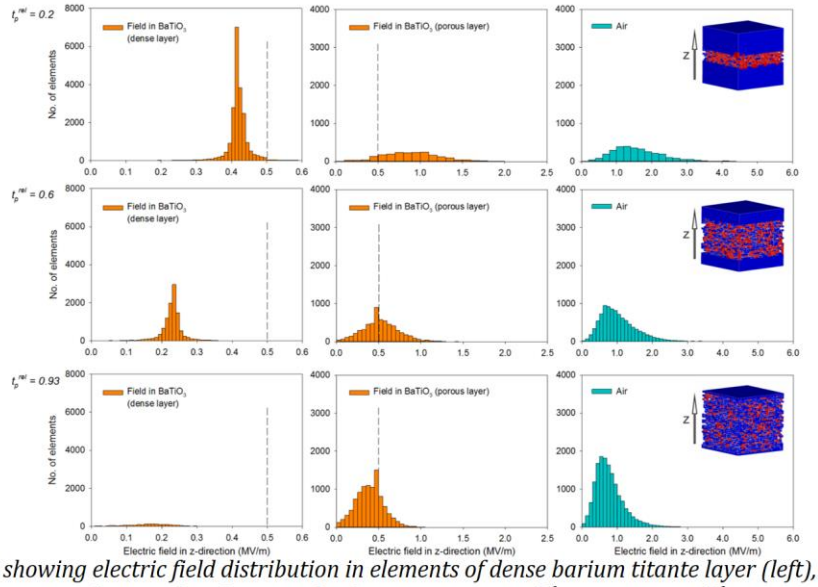

Figure 6: *Histograms showing electric field distribution in elements of dense barium titante layer (left), barium titanate phase in the porous layer (centre) and air (right) for ~60vol.% layer porosity at* $t_p^{rel} = 0.2$ *(top),* $t_p^{rel} = 0.6$ *(middle) and* $t_p^{rel} = 0.93$ *(bottom). The dashed vertical line at 0.5MV/m represents the coercive field,* E_c*, of* $BaTiO_3$*;* $BaTiO_3$ *elements subjected to fields above this line are considered 'poled'. Typical distributions of unpoled* $BaTiO_3$ *elements (blue regions) and poled elements (red regions) are shown for each geometry as insets on the right.*

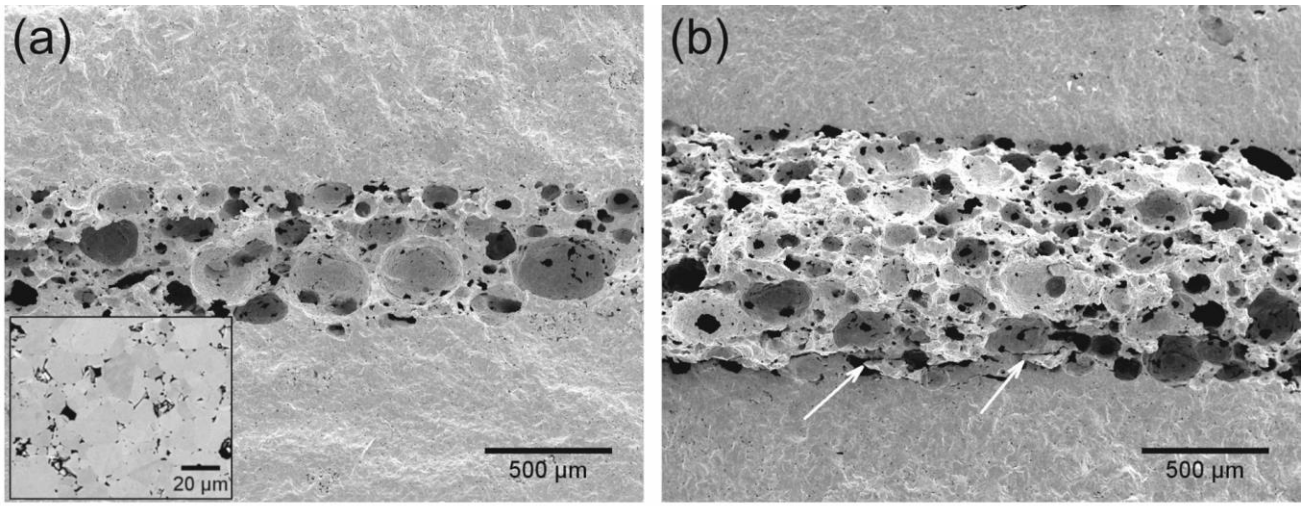

Figure 7: *SEM of fracture surface of cross section of* $BaTiO_3$ *with porous sandwich layer (porosity ~ 60vol.%) with (a) porous layer thickness,* t_p^{rel} *~ 0.25 and relative density ~80%; SEM of dense outer-layer shown as inset, and (b)* t_p^{rel} *~ 0.48, relative density ~66% with small cracks at interface between middle and bottom layers (shown by arrows); the porous layer in this image is on a small angle with respect to the dense layers, which was a common occurrence.*

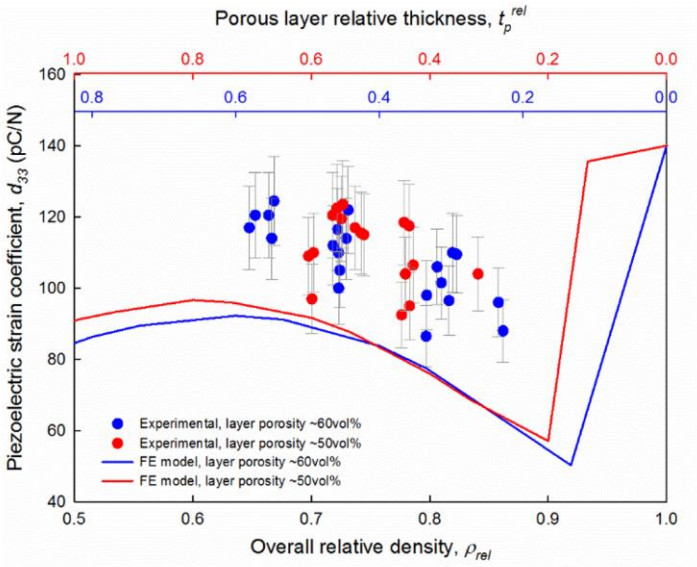

Figure 8: *Comparison of experimental longitudinal piezoelectric coefficient, d_{33}, of $BaTiO_3$ porous sandwich layer structures with FE model. Data is shown across range of overall relative densities for layer porosities of 50 and 60vol.%, in red and blue, respectively. Top axis in gives estimated porous layer relative thickness for corresponding relative density. Error bars at $\pm$10% (accuracy of measurement device).*

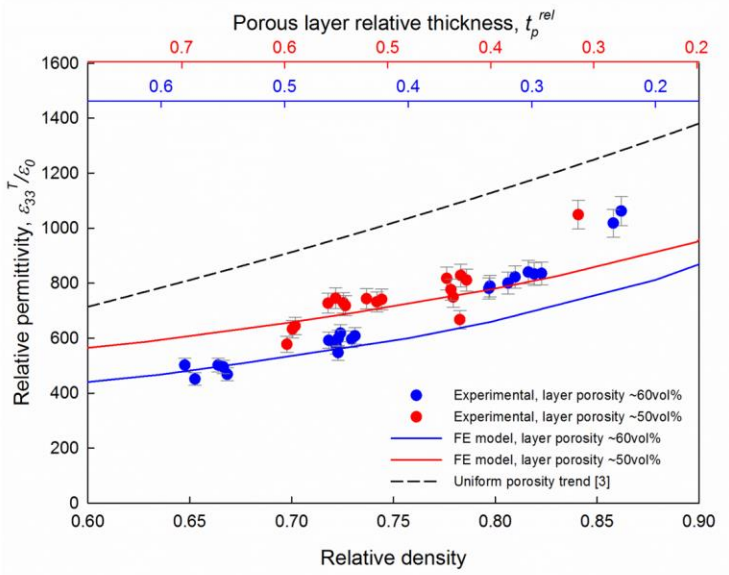

Figure 9: *Comparison of relative permittivity, $\varepsilon_{33}^T/\varepsilon_0$, measured from manufactured porous layer samples (points) with data from FE model (coloured lines) and samples with uniform porosity from previous study (dashed black line) [3]. Data is shown for two layer porosities, 50 and 60vol.%, in red and blue, respectively. Porous layer relative thickness corresponding to layer both layer porosities are on the upper x-axes. Error bars of $\pm$5% are attributed to measurement error of sample dimensions.*

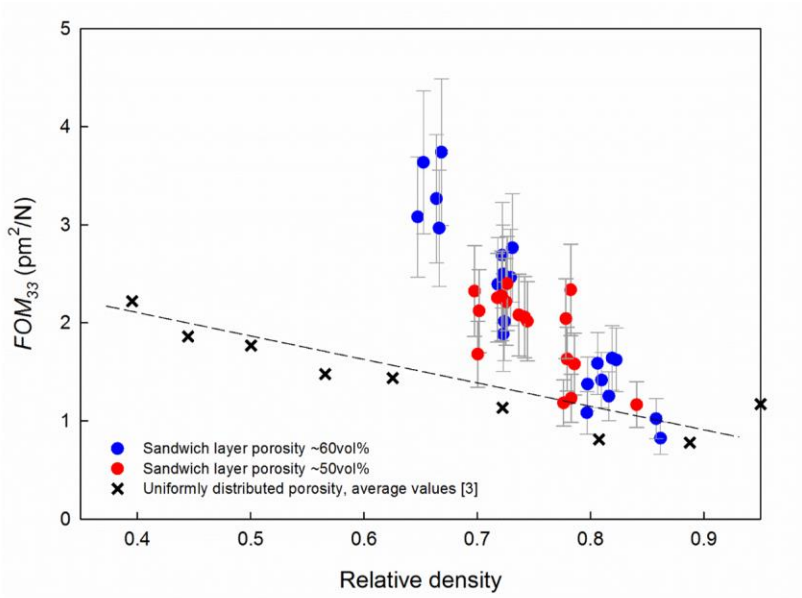

Figure 10: *FOM_{33} ($d_{33}^2/\varepsilon_{33}^T$) for manufactured porous sandwich layer $BaTiO_3$ (red and blue points for 50 and 60vol.% layer porosity, respectively) as a function of relative density. Average values for uniform porous samples from previous study shown for comparison. Dashed black line is an approximate trend of uniform porous data to act as a guide for the eye. Error bars at ±20% (cumulative error).*